



## Thermodynamic Analysis of Silica Refractory Corrosion in Glass-Melting Furnaces

Mark D. Allendorf<sup>a,\*,z</sup> and Karl E. Spear<sup>b,\*\*,\*</sup>

<sup>a</sup>Sandia National Laboratories, Combustion Research Facility, Livermore, California 94551-0969, USA

<sup>b</sup>Department of Materials Science and Engineering, Pennsylvania State University, University Park, Pennsylvania 16802, USA

Corrosion of refractory silica brick used to line the roof or "crown" of many glass-melting furnaces is a serious problem in furnaces using oxygen-fuel rather than air-fuel mixtures. In this work, we report equilibrium calculations that support a corrosion mechanism in which alkali hydroxide gas (NaOH or KOH), produced by reaction of water vapor in the combustion gas with the molten glass, reacts with the silica brick in the furnace crown to produce an alkali silicate liquid with a composition that depends on the temperature of the crown. Our reported calculations predict the variable-composition liquid-solution corrosion product phase as a function of key furnace variables. Critical thermodynamic data needed for the liquid corrosion product were generated using a modified associate species solution model and critical analysis of thermochemical information found in the literature for the Na<sub>2</sub>O-SiO<sub>2</sub> and K<sub>2</sub>O-SiO<sub>2</sub> systems. Excellent agreement with reported Na<sub>2</sub>O-SiO<sub>2</sub> and K<sub>2</sub>O-SiO<sub>2</sub> phase diagrams and with experimentally measured activities for Na<sub>2</sub>O and K<sub>2</sub>O is achieved. The results of our current calculations are for temperatures between 1273 and 1973 K (1000-1700°C) under either air-fired or oxy-fired conditions, and are used to define a "critical temperature," above which corrosion is not expected to occur for a given NaOH(g) or KOH(g) partial pressure.  
© 2001 The Electrochemical Society. [DOI: 10.1149/1.1337603] All rights reserved.

Manuscript submitted July 28, 2000; revised manuscript received October 13, 2000.

Refractory brick composed primarily of silica is commonly used to line the interiors of glass-melting furnaces. In air-fired furnaces, the furnace roof or "crown" typically lasts on the order of ten years. Recently, however, the replacement of air with pure oxygen in the combustion gases in many melting furnaces has led to substantially higher silica corrosion rates.<sup>1</sup> In some cases, crown lifetimes decreased by as much as a factor of two. The high cost of rebuilding these furnaces is driving organized efforts to determine the factors controlling corrosion, so that either furnace conditions can be adjusted to reduce corrosion to acceptable rates or alternative refractory materials can be identified that are more inert. The former solution is preferable since silica brick is attractive because of its low density (which simplifies furnace construction), low thermal conductivity, and low cost.

A major component of many glasses is sodium oxide (Na<sub>2</sub>O), which in the presence of combustion-generated water vapor forms gas-phase sodium hydroxide (NaOH). Some glasses, such as those used to make television tubes and lead "crystal" tableware, also contain high concentrations of potassium oxide (K<sub>2</sub>O), which reacts with water vapor to form potassium hydroxide (KOH). Reaction of these hydroxide gases with the silica brick in the furnace crown to produce an alkali silicate liquid is assumed to be the corrosion mechanism (Fig. 1), based on postmortem analysis of refractory samples.<sup>2,3</sup> Experimental concentrations of NaOH(g) in oxy-fuel furnaces are reported to be as much as three to four times higher than in air-fired furnaces.<sup>2</sup> Both temperature<sup>4</sup> and gas velocity<sup>5</sup> also appear to play important roles. Since the temperatures of the silica refractory are typically quite high, ranging from more than 1600°C at the surface exposed to the furnace to above 1100°C on the exterior side of an insulated crown, equilibrium represents a reasonable description of the chemical behavior of the corrosion processes. Thus, thermodynamic calculations that predict equilibrium chemical compositions can play a useful role by identifying energetically stable species and by predicting the limiting extent of corrosion and corrosion products.

Previous investigators have used calculations of equilibria in the Na<sub>2</sub>O-SiO<sub>2</sub><sup>4,6,7</sup> and K<sub>2</sub>O-SiO<sub>2</sub><sup>6</sup> systems to identify gas-phase species present in furnace atmospheres and to examine the dependence of the SiO<sub>2</sub> corrosion by alkali hydroxides on refractory temperature,

and NaOH(g) concentration, and water vapor concentration. However, these calculations did not consider the formation of any variable-composition liquid-silicate phases. As a result, there may be systematic errors in the conclusions deduced from these previous results.

The accuracy of a thermodynamic calculation depends, of course, on the quality and completeness of the data employed. Unfortunately, the M<sub>2</sub>O-SiO<sub>2</sub> systems are quite complex and very high deviations from Raoult's law are observed with the use of typical liquid solution models. Methods that attempt to model nonideal solution behavior are needed to determine accurate thermodynamic functions for the low-melting glass that are the typical products of silica corrosion by alkali-containing species. The thermodynamics of the sodium oxide/silica system have been extensively studied due to their importance in a variety of fields; two recent investigations by Wu *et al.*<sup>8</sup> and Zaitsev *et al.*<sup>9</sup> provide the latest experimental data for these systems as well as reviews of the relevant literature. Wu *et al.* fit the Na<sub>2</sub>O-SiO<sub>2</sub> and K<sub>2</sub>O-SiO<sub>2</sub> phase diagrams using their "quasi-chemical" model of the liquid phase to obtain the activities of Na<sub>2</sub>O and K<sub>2</sub>O in melts with SiO<sub>2</sub>; the results are in good agreement with experiment. Zaitsev *et al.* used Knudsen effusion mass spectrometry to determine Na<sub>2</sub>O and SiO<sub>2</sub> activities in the melt as a

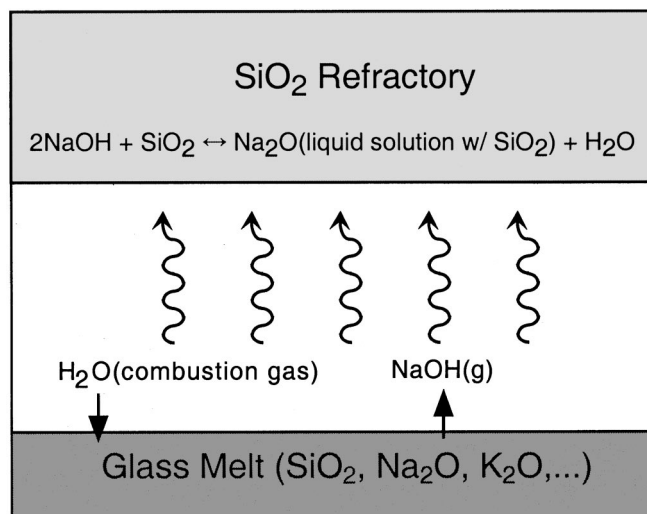


**Figure 1.** Schematic of the processes involved in the corrosion of silica refractory by NaOH(g).

\* Electrochemical Society Active Member.

\*\* Electrochemical Society Fellow.

<sup>z</sup> E-mail: mdallen@sandia.gov

**Table I. Typical input conditions for equilibrium calculations.  $P(\text{total})=1$  bar,  $T = 1200\text{--}2000$  K (927–1727°C).**

	$n(\text{CH}_4)^a$	$n(\text{O}_2)^a$	$n(\text{N}_2)^a$	$n(\text{M}_2\text{O})^{a,c}$	$a(\text{SiO}_2)^b$
Calculation of $p_{\text{H}_2\text{O}}$					
Air-fired fuel mixture	1.00	2.05	8.2	-	-
Oxy-fired fuel mixture	1.00	2.05	-	-	-
Corrosion predictions					
Air-fired fuel mixture	1.00	2.05	8.2	0.1	1.0
Oxy-fired fuel mixture	1.00	2.05	-	0.1	1.0

<sup>a</sup> Moles.<sup>b</sup> Activity of  $\text{SiO}_2$  (crystalline) was fixed at unity.<sup>c</sup> M = Na or K.

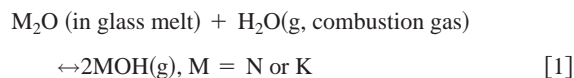
function of composition and temperature, as well as thermodynamic functions for the  $\text{Na}_2\text{O}\text{--}\text{SiO}_2$  melt and of solid silicates at high-temperature. These investigators also provide a thorough comparison of their results with the available data in the literature for this system.

In this work, we use a modified associate species model<sup>10</sup> to describe the thermodynamic functions for the liquid phases in the  $\text{Na}_2\text{O}\text{--}\text{SiO}_2$  and  $\text{K}_2\text{O}\text{--}\text{SiO}_2$  systems. We then use these data to calculate the equilibrium between silica and typical air- and oxy-fuel-fired glass-melting atmospheres. These are the first calculations to assess the impact of the formation of sodium- or potassium-silicate glasses on the corrosion of silica. The corrosion results reported here include (i) the temperature dependence of gas-phase alkali-containing species concentrations in equilibrium with a liquid corrosion product and crystalline  $\text{SiO}_2$ ; (ii) the composition of the corrosion products and their temperature dependence; and (iii) the predicted refractory temperature and MOH furnace concentration regimes in which corrosion of silica is expected to occur. Finally, we use these results to suggest mechanisms that may be active in the corrosion process. A preliminary report of our work on the corrosion of silica refractories by sodium-containing species was given in a proceedings volume.<sup>11</sup> However, a more thorough analysis and listing of the thermodynamic data for the  $\text{Na}_2\text{O}\text{--}\text{SiO}_2$  system, including the liquid  $\text{Na}_2\text{O}\text{--}\text{SiO}_2$  phase, and refined predictive results for the silica refractory corrosion are reported in the present paper.

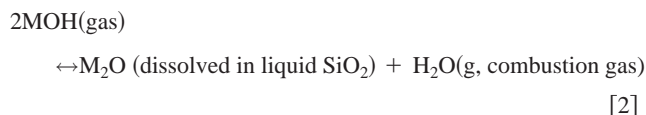
### Corrosion Mechanisms, Thermodynamic Data, and Modeling Approach

*Corrosion reactions.*—Previous calculations<sup>6,11</sup> as well as those reported here show that  $\text{NaOH}(\text{g})$  and  $\text{KOH}(\text{g})$  are the most abundant gaseous species containing alkali metals at equilibrium between combustion atmospheres and sodium- or potassium-containing glass melts. Therefore, we assume in these calculations that  $\text{MOH}(\text{g})$  is

the key alkali-containing species participating in the corrosion of silica. Its formation can be described by the following chemical reaction



At the surface of the refractory, a second reaction occurs to form a silica-rich liquid solution in which  $\text{M}_2\text{O}$  is dissolved



The liquid  $\text{SiO}_2$  solution in Reaction 2 is in equilibrium with crystalline  $\text{SiO}_2$  (cristobalite above  $\sim 1470^\circ\text{C}$ ). This liquid solution composition is fixed by the temperature of the liquid- $\text{SiO}_2$  (crystalline) equilibrium shown at high temperatures in the  $\text{SiO}_2$ -rich regions of the binary  $\text{M}_2\text{O}\text{--}\text{SiO}_2$  phase diagrams discussed below. The fixed composition at a given temperature translates to a fixed activity of  $\text{M}_2\text{O}$  in the liquid solution at this temperature. Since the partial pressure of water is determined by the furnace atmosphere (mostly the combustion equilibria), and  $K_{\text{eq}}(2)$  is a constant at a given temperature, only one partial pressure of  $\text{MOH}(\text{g})$  can exist in equilibrium with the silica refractory and its liquid corrosion product at the temperature of the refractory surface. If the partial pressure of  $\text{MOH}(\text{g})$  produced by Reaction 1 is smaller than the equilibrium value for Reaction 2, no corrosion will occur; conversely if the partial pressure of  $\text{MOH}(\text{g})$  from Reaction 1 is larger than that at equilibrium for Reaction 2, this latter reaction is driven to the right

**Table II. Major species used in calculations and sources of thermodynamic data.**

Gas phase <sup>a</sup>					
$\text{N}_2$	$\text{N}_2\text{O}$	$\text{NO}$	$\text{NO}_2$	$\text{O}_2$	$\text{H}_2$
$\text{H}$	$\text{OH}$	$\text{H}_2\text{O}$	$\text{CH}_4$	$\text{CO}$	$\text{CO}_2$
$\text{NH}_3$	$\text{HCN}$	$\text{SiO}_2$	$\text{SiO}$		
$\text{Na}$	$\text{NaOH}^b$	$\text{K}$	$\text{KOH}$		
Liquid phase <sup>c</sup>					
$\text{Na}_2\text{O}(1)$	$(2/5)\text{Na}_4\text{SiO}_4$	$(2/3)\text{Na}_3\text{SiO}_3$	$(1/2)\text{Na}_3\text{Si}_2\text{O}_5$	$\text{Si}_2\text{O}_4$	
$\text{K}_2\text{O}(1)$	$(2/3)\text{K}_2\text{SiO}_3$	$(1/2)\text{K}_2\text{Si}_2\text{O}_5$	$(1/3)\text{K}_2\text{Si}_4\text{O}_9$		
Solid phases <sup>c</sup>					
$\text{SiO}_2$ (cristobalite)	$\text{SiO}_2$ (tridymite)	$\text{SiO}_2$ (quartz)			
$\text{Na}_2\text{O}$	$\text{Na}_4\text{SiO}_4$	$\text{Na}_6\text{Si}_2\text{O}_7$	$\text{Na}_2\text{SiO}_3$	$\text{Na}_2\text{Si}_2\text{O}_5$	$\text{Na}_6\text{Si}_8\text{O}_{19}$
$\text{K}_2\text{O}$	$\text{K}_2\text{SiO}_3$	$\text{K}_2\text{Si}_2\text{O}_5$	$\text{K}_2\text{Si}_4\text{O}_9$		

<sup>a</sup> A total of 75 species were initially used in these calculations. The major source of their thermodynamic data was SGTE (Ref. 14 except as noted).<sup>b</sup> Thermodynamic data from JANAF (Ref. 15).<sup>c</sup> The source of thermodynamic data for the listed liquid and solid species was assessments of the type described in Ref. 10; values for these species are listed in Table III. A total of 15 fixed composition solid phases were initially included in our data file, but only the above phases were of importance for the present study.

Table III. Thermodynamic data for important species in Na<sub>2</sub>O-SiO<sub>2</sub> and K<sub>2</sub>O-SiO<sub>2</sub> systems.

Species	$\Delta H_{f,298}^\circ$ (J/mol)	$S_{298}^\circ$ (J/mol-K)	T(K)	$C_p = a + b \cdot T + c \cdot T^2 + d/T^2$ (J/mol-K)			
				<i>a</i>	<i>b</i> · 10 <sup>3</sup>	<i>c</i> · 10 <sup>6</sup>	<i>d</i> · 10 <sup>-5</sup>
Gases							
Na	107,500	153.716	2700	21.025	-0.384	0.143	-0.134
			4700	61.372	0.445	-0.052	-31.192
NaOH <sup>a</sup>	-197,757	228.443	1500	51.971	2.281	0.778	-3.848
			6000	58.196	1.315	-0.115	-66.087
K	89,000	160.339	2100	21.136	-0.653	0.293	-0.017
			4500	16.475	-0.366	0.709	9.801
KOH	-232,630	236.376	1200	53.038	-0.004	2.094	-4.168
			3200	52.639	4.546	-0.614	-20.879
Liquid associates							
Na <sub>2</sub> O(1)	-370,284	108.989	1023	55.480	70.210	-30.540	-4.140
	$\Delta H_{trans}^\circ$ (1023 K) = 1,757		1243	82.563	12.350	0	0
	$\Delta H_{trans}^\circ$ (1243 K) = 11,924		1405	82.563	12.350	0	0
			3500	104.600	0	0	0
Na <sub>4</sub> SiO <sub>4</sub> (2/5)	-785,540	117.004	1000	73.036	56.920	-24.436	-18.936
			1393	94.702	10.632	0	-15.624
			3000	112.332	0.752	0	-15.624
Na <sub>2</sub> SiO <sub>3</sub> (2/3)	-980,800	116.366	1000	84.740	48.060	-20.360	-28.800
			1363	102.795	9.487	0	-26.040
			3000	117.487	1.253	0	-26.040
Na <sub>2</sub> Si <sub>2</sub> O <sub>5</sub> (/2)	-1,199,000	113.875	1147	99.370	36.985	-15.270	-41.130
			3000	123.930	1.880	0	-39.060
K <sub>2</sub> O(1)	-327,300	129.959	1013	75.947	17.146	0	-5.196
			3000	100.000	0	0	0
K <sub>2</sub> SiO <sub>3</sub> (2/3)	-997,100	123.100	1249	98.385	12.684	0	-29.984
			3000	114.420	1.253	0	-26.040
K <sub>2</sub> Si <sub>2</sub> O <sub>5</sub> (/2)	-1,220,370	117.100	1319	109.604	10.453	0	-42.018
			3000	121.630	1.880	0	-39.060
K <sub>2</sub> Si <sub>4</sub> O <sub>9</sub> (/3)	-1,425,750	106.300	1043	120.822	8.222	0	-54.052
			3000	128.840	2.507	0	-52.080
Si <sub>2</sub> O <sub>4</sub> (1)	-1,793,592	101.658	1996	143.260	3.760	0	-78.120
			3000	171.544	0	0	0
Crystalline solids							
Na <sub>2</sub> O	-417,982	75.040	1023	55.480	70.210	-30.540	-4.140
	-417,982 <sup>b</sup>	75.061 <sup>b</sup>					
	$\Delta H_{trans}^\circ$ (1023 K) = 1,757		1243	82.563	12.350	0	0
	$\Delta H_{trans}^\circ$ (1243 K) = 11,924		2500	82.563	12.350	0	0
Na <sub>4</sub> SiO <sub>4</sub>	-2,095,630	195.811	1000	182.590	142.300	-61.080	-47.340
	-2,101,297	195.811	1393	236.756	26.580	0	-39.060
			3000	280.830	1.880	0	-39.060
Na <sub>6</sub> Si <sub>2</sub> O <sub>7</sub>	-3,676,200	317.000	1000	309.700	214.390	-91.620	-90.540
	-3,596,080	360.826	1363	390.949	40.810	0	-78.120
			3000	457.060	3.760	0	-78.120
Na <sub>2</sub> SiO <sub>3</sub>	-1,555,500	119.000	1000	127.110	72.090	-30.540	-43.200
	-1,558,601	113.846	1363	154.193	14.230	0	-39.060
			3000	176.230	1.880	0	-39.060
Na <sub>2</sub> Si <sub>2</sub> O <sub>5</sub>	-2,475,200	165.000	1147	198.740	73.970	-30.540	-82.260
	-2,470,340	164.055	3000	247.860	3.760	0	-78.120
Na <sub>6</sub> Si <sub>8</sub> O <sub>19</sub>	-9,241,573	585.000	1147	739.480	225.670	-91.620	-324.900
	-9,167,917	652.863	3000	886.84	15.040	0	-312.480
K <sub>2</sub> O	-361.700	96.000	1013	75.947	17.1460	0	-5.196
	-361.498	102.006	3000	100.000	0	0	0
K <sub>2</sub> SiO <sub>3</sub>	-1,544,000	146.000	1249	147.577	19.0260	0	-44.976
	-1,560,362	146.147	3000	171.630	1.8800	0	-39.060
K <sub>2</sub> Si <sub>2</sub> O <sub>5</sub>	-2,509,000	191.000	1319	219.207	20.906	0	-84.036
	-2,522,542	182.004	3000	243.260	3.760	0	-78.120
K <sub>2</sub> Si <sub>4</sub> O <sub>9</sub>	-4,327,000	282.000	1043	362.467	24.6660	0	-162.156
	-4,338,562	265.684	3000	386.520	7.5200	0	-156.240
SiO <sub>2</sub> (cris)	-906,377	46.029	1996	71.630	1.880	0	-39.060
	-906,377	46.029	3000	85.772	0	0	0
SiO <sub>2</sub> (trid)	-907,257	45.524	1996	71.630	1.880	0	-39.060
	-907,045	45.524	3000	85.772	0	0	0
SiO <sub>2</sub> (quar)	-908,758	44.207	1996	71.630	1.880	0	-39.060
	-908,627	44.207	3000	85.772	0	0	0

<sup>a</sup> Data from JANAF Tables,<sup>15</sup> see text for discussion of uncertainties in NaOH(g) data.<sup>b</sup> Values for  $\Delta H_{f,298}^\circ$  and  $S_{298}^\circ$  in *italics* are from Wu *et al.*<sup>8</sup>

**Table IV. Excess free energy equations representing the positive interaction terms between pairs of liquid associate species in liquid solutions. A Redlich-Kister expansion of a regular solution constant is used.**

$\text{Na}_2\text{Si}_2\text{O}_5(1/2)\text{-Si}_2\text{O}_4(1)$	$\Delta G^{\text{exs}} = X(1-X) \{10,000 - 11,400(1-2X)\}$	(J/mol of liquid species)
$\text{K}_2\text{Si}_4\text{O}_9(1/3)\text{-Si}_2\text{O}_4(1)$	$\Delta G^{\text{exs}} = X(1-X) \{14,000 - 3,800(1-2X)\}$	(J/mol of liquid species)

and corrosion occurs. Therefore, to model the above corrosion reactions at equilibrium requires knowledge of the partial pressure of  $\text{H}_2\text{O}(\text{g})$  ( $p_{\text{H}_2\text{O}}$ ) in the combustion atmosphere and the activity of  $\text{M}_2\text{O}$  ( $a_{\text{M}_2\text{O}}$ ) as a function of temperature and composition in the  $\text{SiO}_2$ -rich liquid that is in equilibrium with crystalline  $\text{SiO}_2$ . The equilibrium constants  $K_{\text{eq}}$  for Reactions 1 and 2 as a function of temperature are also needed, but note that  $K_{\text{eq}}(1) = [1/K_{\text{eq}}(2)]$ .

*Computational approach to equilibrium modeling of the furnace-gas/refractory interaction.*—Although the equilibrium temperature of the combustion gases could be predicted by performing an equilibrium calculation under the constraints of constant enthalpy and pressure, the adiabatic flame temperature thus obtained is not an accurate reflection of the true furnace-gas temperature. This is due to the fact that heat losses in the furnace, which are difficult to predict, play a critical role in determining the actual temperature of the combustion gases. Consequently, we performed our calculations under the constraints of constant temperature and pressure. A range of temperatures was used (1200–2000 K) that could be encountered by the refractory. All calculations were performed for a total pressure of 1 bar. Recall that, while temperatures at the refractory surface may be quite high ( $\sim 1900$  K), large temperature gradients, amounting to hundreds of degrees over a distance of roughly 30 cm, can exist within the silica brick (see Introduction). Since these refractories are porous ( $\sim 20$ – $25\%$  is typical), combustion gases can permeate the brick and encounter substantially lower temperatures. The partial pressure of  $\text{H}_2\text{O}$  in the combustion gas,  $p_{\text{H}_2\text{O}}$ , which plays a key role in the corrosion process (Reactions 1 and 2), is thus (primarily) determined by the input fuel/oxygen ratio used in the calculations. The input compositions used are given in Table I.

*Thermodynamic data.*—To be able to predict the corrosion of crystalline silica, reliable high-temperature thermodynamic and phase-equilibria data are required for all critical species and phases in the  $\text{M}_2\text{O}$ - $\text{SiO}_2$ - $\text{H}_2\text{O}$  system. These data are available for most of the combustion gases involved, although the range in reported values for the heat of formation for NaOH is relatively large, as is discussed below. Table II provides a listing of major species used in the calculations, and their sources of thermodynamic data. Tabulated data for liquid-phase corrosion products are lacking, so these values were determined as part of an assessment and optimization of the values for all liquid and crystalline phases in the  $\text{M}_2\text{O}$ - $\text{SiO}_2$  binary systems. The computer program ChemSage,<sup>12,13</sup> was the primary tool used for developing an assessed, internally consistent thermodynamic database for the  $\text{Na}_2\text{O}$ - $\text{SiO}_2$  and  $\text{K}_2\text{O}$ - $\text{SiO}_2$  systems, and for performing subsequent calculations of the high-temperature corrosion reactions between  $\text{MOH}(\text{g})$  and  $\text{SiO}_2(\text{s})$ . The following paragraphs describe our analysis of the available data for this system and the choices made for the values used in the equilibrium calculations described later in this paper.

The required thermodynamic data for most gas-phase species were obtained from the assessed SGTE database.<sup>14</sup> However, the  $\Delta H_{\text{f},298}^\circ$  value for  $\text{NaOH}(\text{g})$  in this database ( $-185.649$  kJ/mol) is quite different from that found in the *JANAF Thermochemical Tables* ( $-197.757$  kJ/mol),<sup>15</sup> although the corresponding values of the entropy ( $S_{298}^\circ$ ) from the two sources are quite similar (228.589 and 228.443 J/mol-K, respectively). The  $\Delta H_{\text{f},298}^\circ$  and  $S_{298}^\circ$  values for the solid,  $\text{NaOH}(\text{s})$ , from the two sources are essentially the same. Thus, the 12 kJ/mol difference in the  $\Delta H_{\text{f},298}^\circ$  values for the vapor species appears to be the only major uncertainty in the sodium hydroxide data used in our calculations. Communications with the

Russian group responsible for the IVANTHERMO database (Gorokhov *et al.*)<sup>16</sup> revealed that their experimental mass-spectrometric measurements of NaOH vapor pressures yield a  $\Delta H_{\text{f},298}^\circ$  of  $-189.7 \pm 4$  kJ/mol. The IVANTHERMO Database<sup>17</sup> has assessed this value to be  $-191.0 \pm 8$  kJ/mol. Both of these values lie between the SGTE and JANAF values. In the calculations described here, we use the JANAF value for  $\Delta H_{\text{f},298}^\circ(\text{NaOH}, \text{g})$ . However, the effect of the difference in the SGTE and JANAF values in predicting the critical boundary lines that separate corrosive from noncorrosive conditions for air-fired and oxygen-fired furnaces is included and discussed later in Fig. 9.

The thermodynamic data for the binary  $\text{Na}_2\text{O}$ - $\text{SiO}_2$  and  $\text{K}_2\text{O}$ - $\text{SiO}_2$  systems, including their liquid phases, were assessed and optimized by performing a CALPHAD-type thermodynamic fitting of the binary equilibrium phase diagrams for these systems. As described previously,<sup>10</sup> this procedure provides a means of testing and generating a set of self-consistent thermodynamic information for a system, including the generation of thermodynamic data for the oxide liquid phase. Data for the phase diagrams such as phase formation, melting points, eutectic compositions, and liquidus curves were obtained from various sources (primarily from *Phase Diagrams for Ceramists*,<sup>18</sup> Wu *et al.*,<sup>8</sup> and Zaitsev *et al.*<sup>9</sup>; the latter two papers provide an extensive critical assessment of the available data). Experimental activity data for  $\text{M}_2\text{O}(\text{l})$  in the  $\text{M}_2\text{O}$ - $\text{SiO}_2$  liquid phases for  $\text{M} = \text{Na}$ <sup>8,9,19-23</sup> and  $\text{M} = \text{K}$ <sup>8,24-26</sup> are available from a wide range of sources and are compared with calculated values in the Results section of this paper.

Accurate values of the thermodynamic data for liquid-oxide solutions are of critical importance to our thermodynamic description of the  $\text{M}_2\text{O}$ -containing liquid corrosion product. To obtain these values, we described the liquid using a modified associate species model that has been previously discussed.<sup>10</sup> This model uses intermediate liquid chemical species with their corresponding thermodynamic data to represent the negative free-energy terms caused by nonideal mixing of the end-member components in a system. For example, in the  $\text{Na}_2\text{O}$ - $\text{SiO}_2$  binary system, the liquid is composed of liquid species  $\text{Na}_2\text{O}$ ,  $(2/5)\text{Na}_4\text{SiO}_4$ ,  $(2/3)\text{Na}_2\text{SiO}_3$ ,  $(1/2)\text{Na}_2\text{Si}_2\text{O}_5$ , and  $\text{Si}_2\text{O}_4$ . Table III provides a complete listing of associate species used in the current calculations. To provide equal weighting to all liquid associate species, each species contains a total of two non-oxygen atoms in its formula. While these liquid species may not exist as chemical entities that can be isolated and characterized, they can accurately represent the negative interaction energies that occur between  $\text{M}_2\text{O}$  and  $\text{SiO}_2$  at specific compositions in this liquid oxide solution. Positive interactions (repulsion terms ultimately leading to phase separation in solutions) cannot be modeled using the standard associate species model. Instead, we use positive interaction parameters between pairs of associate species that compositionally bound the region of phase separation (immiscibility gap).<sup>10</sup> In the two chemical systems of interest in this paper, these respective pairs of species are  $(1/2)\text{Na}_2\text{Si}_2\text{O}_5$  and  $\text{Si}_2\text{O}_4$ , and  $(1/3)\text{K}_2\text{Si}_4\text{O}_9$  and  $\text{Si}_2\text{O}_4$ . A composition-dependent regular solution constant is used in representing the excess free energy. The excess free energy equations and constants for these two interactions are given in Table IV. These equations accurately model the liquid thermodynamics in the composition region in which a metastable immiscibility gap has been reported for glass phases in these systems (see the lower right por-

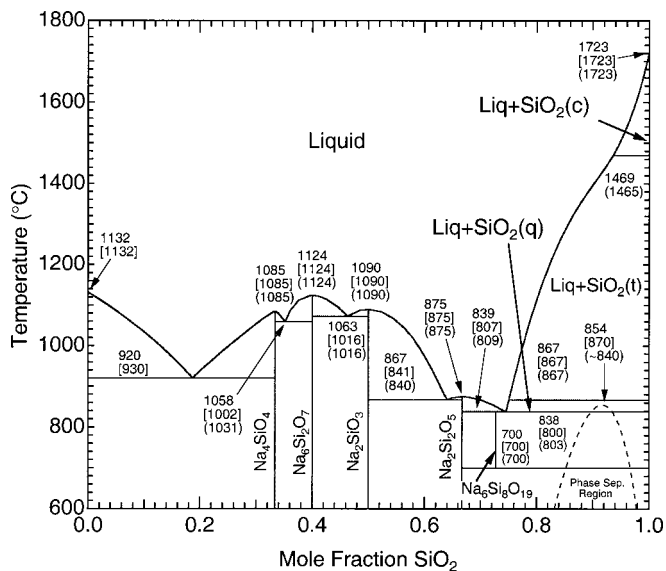


**Figure 2.** Calculated phase diagram for the Na<sub>2</sub>O-SiO<sub>2</sub> system. Current temperatures are shown, along with previously reported values in parentheses (Ref. 8) and brackets (Ref. 9).

tions of the phase diagrams in Fig. 2 and 4). The thermodynamic data for the system was optimized to achieve the best overall agreement with the most accurate experimental information reported for (i) each phase, (ii) the phase diagram, and (iii) experimentally measured activities for Na<sub>2</sub>O and K<sub>2</sub>O dissolved in liquid silica.

The set of thermodynamic data we used for all condensed species and the important gas-phase species in the Na<sub>2</sub>O-SiO<sub>2</sub> and K<sub>2</sub>O-SiO<sub>2</sub> systems are listed in Table III. The data in this table are in a form directly usable by ChemSage, and were used to calculate the phase diagrams shown in Fig. 2 and 4,<sup>c</sup> and the activity plots shown in Fig. 3 and 5. These data include  $\Delta H_{f,298}^\circ$  and  $S_{298}^\circ$  values, along with  $C_p$  equations for various temperature ranges, and enthalpies of

<sup>c</sup> Temperatures in these figures are given in degrees Celsius for ease of comparison with the referenced phase diagrams in the literature. Units of kelvin are used in the remainder of the discussion.

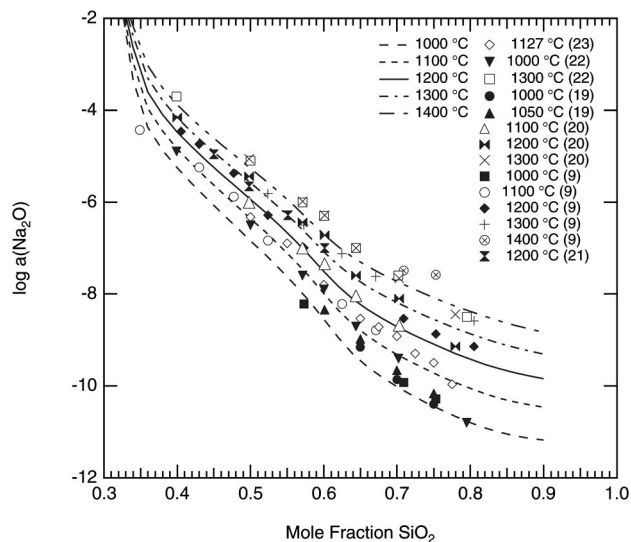


**Figure 3.** Calculated and measured (Ref. 8, 9, 19-23) Na<sub>2</sub>O activities in Na<sub>2</sub>O-SiO<sub>2</sub> liquid (glass) solutions.

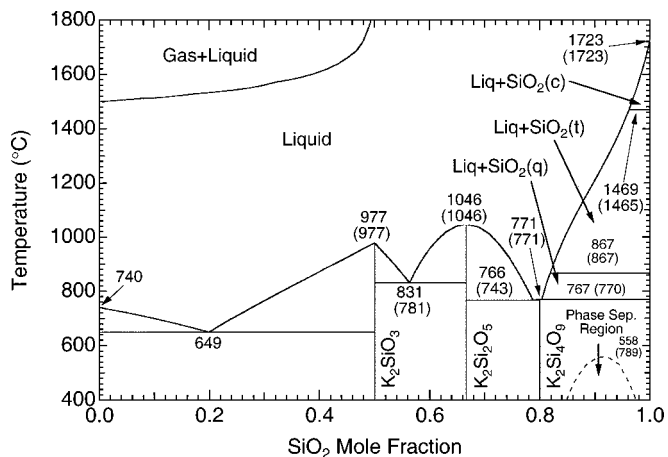


**Figure 4.** Calculated phase diagram for the K<sub>2</sub>O-SiO<sub>2</sub> system. Current temperatures are shown, along with previously reported values in parentheses (Ref. 8).

phase transformations when appropriate. Enthalpies of fusion are not listed separately since these numbers are incorporated in the relative enthalpies of formation of liquid and solid phases. The positive interaction parameters for the pairs of liquid species bounding metastable liquid immiscibility gaps are also given in this table in the form of excess free energies of solution. The agreement with reported information and our calculated diagrams and activities is quite good, as is discussed below.

*Modeling the M<sub>2</sub>O-SiO<sub>2</sub> phase diagram and M<sub>2</sub>O activities.*— To model the corrosion of silica refractories, we first determined thermodynamic data given in Table III for sodium-containing and potassium-containing silica-rich liquid phases that exist in equilibrium with crystalline silica. These liquids are the expected products of silica corrosion by NaOH(g) and KOH(g). We used the above-mentioned modified associate species model to represent the liquid solution thermodynamic behavior. The results of these calculations are shown in the form of a phase diagram for the Na<sub>2</sub>O-SiO<sub>2</sub> system<sup>c</sup> in Fig. 2, and for the K<sub>2</sub>O-SiO<sub>2</sub> system<sup>c</sup> in Fig. 4.

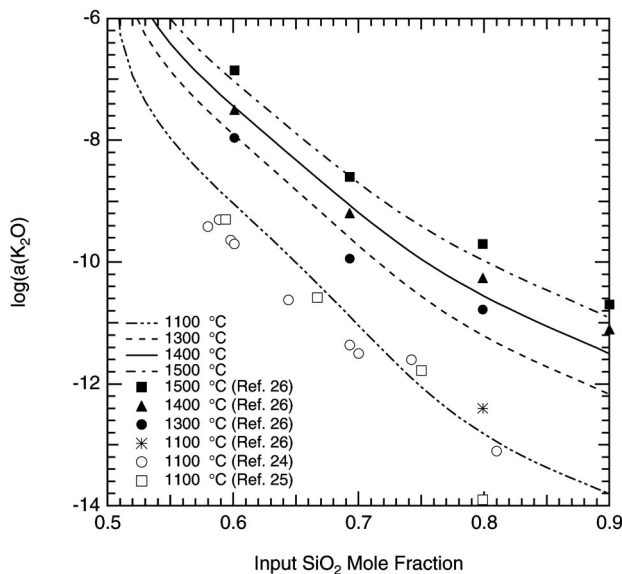


**Figure 5.** Calculated and measured (Ref. 8, 24-26) K<sub>2</sub>O activities in K<sub>2</sub>O-SiO<sub>2</sub> liquid (glass) solutions.

Predicted melting points and eutectic compositions are given in each figure; numbers in parenthesis<sup>8</sup> and square brackets<sup>9</sup> correspond to reported values. The Na<sub>2</sub>O-SiO<sub>2</sub> diagram is in good agreement with the experimental and assessed phase diagram for the well-established crystalline phases of Na<sub>4</sub>SiO<sub>4</sub>, Na<sub>6</sub>SiO<sub>7</sub>, Na<sub>2</sub>SiO<sub>3</sub>, Na<sub>2</sub>Si<sub>2</sub>O<sub>5</sub>, Na<sub>6</sub>Si<sub>8</sub>O<sub>19</sub> and given by Wu *et al.*,<sup>8</sup> and Zaitsev *et al.*<sup>9</sup> The calculated phase diagram for the K<sub>2</sub>O-SiO<sub>2</sub> system given in Fig. 4 agrees well with the critically assessed diagram given by Wu *et al.*<sup>8</sup>

The important portions of these diagrams for this corrosion study are the two-phase regions in which crystalline silica (either cristobalite or tridymite) is in equilibrium with a liquid of composition [(M<sub>2</sub>O)<sub>1-x</sub>(SiO<sub>2</sub>)<sub>x</sub>, where X(SiO<sub>2</sub>) ≥ 0.8]. The thermodynamic data for the SiO<sub>2</sub>-rich liquids in the two alkali systems predict the observed metastable liquid-phase separations (immiscibilities) that occur for X(SiO<sub>2</sub>) > 0.8 portion of the diagrams at temperatures below about 855°C for the Na<sub>2</sub>O-SiO<sub>2</sub> system, and at temperatures below about 558°C for the K<sub>2</sub>O-SiO<sub>2</sub> system. Calculated phase transition temperatures for SiO<sub>2</sub>(s) using the data in Table III also agree well with reported values.

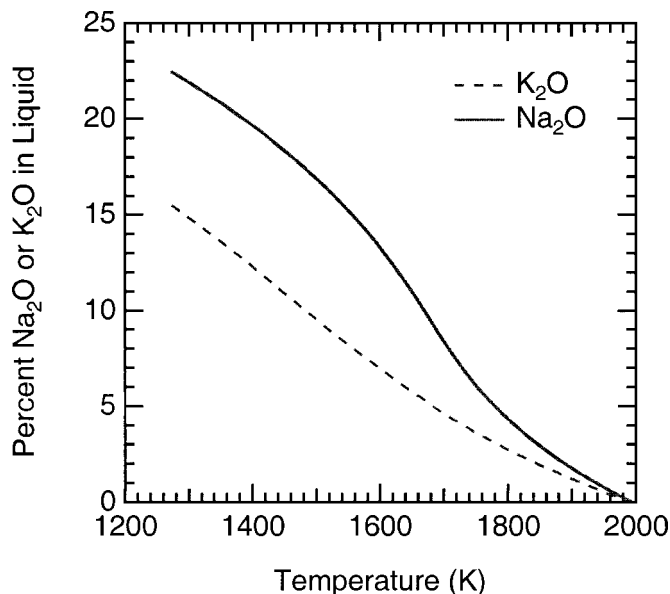
As shown in Fig. 3 and 5, our use of the modified associate species model for the liquid phase (glass), and our assessed thermodynamic properties for this phase are in good agreement with measured values of the activities of M<sub>2</sub>O (*a*<sub>M<sub>2</sub>O</sub>) dissolved in liquid silica (M = Na or K). Significant scatter exists in the reported values, but this is not unexpected considering the difficulty in making such measurements on well-characterized samples at well-defined temperatures. The combined agreement of our calculated and reported activity values, and our calculated and reported binary phase diagrams for the two M<sub>2</sub>O-SiO<sub>2</sub> systems provides a stringent test of the relative accuracy and internal consistency of the sets of thermodynamic data given in Table III.

### Corrosion Analysis, Predictions, and Discussion: Equilibrium Predictions of Silica Corrosion by Na- or K-Containing Species

The phase diagrams for the Na<sub>2</sub>O-SiO<sub>2</sub> and K<sub>2</sub>O-SiO<sub>2</sub> systems in Fig. 2 and 4, respectively, reveal that at the temperatures in the glass melting furnaces, crystalline silica in the refractory can react with Na- or K-containing species to produce an equilibrium product consisting of a silica-rich liquid containing dissolved Na<sub>2</sub>O or K<sub>2</sub>O. Although crystalline alkali silicates are included in the calculations (Table II), none are predicted to form in the temperature range of the glass furnaces. Figure 6 shows that the respective Na<sub>2</sub>O and K<sub>2</sub>O mole fraction (*X*<sub>M<sub>2</sub>O</sub>) in the liquid corrosion product decreases from values greater than 0.15 at ≤1200 K to zero at 1996 K, the melting point of cristobalite. This changing M<sub>2</sub>O concentration with temperature in liquids that equilibrate with crystalline SiO<sub>2</sub> has two important consequences for the development of corrosion mechanisms. First, the minimum partial pressures of MOH(g) that can cause corrosion depend on the activity of M<sub>2</sub>O in the liquid corrosion product (and thus the composition of this liquid). Second, it is known that increasing M<sub>2</sub>O concentrations in the liquid corrosion product reduces the viscosity of alkali silicate melts.<sup>27,28</sup>

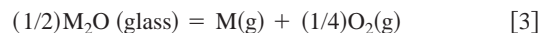
Selected results of equilibrium calculations for two typical combustion mixtures (see Table I) are shown in Fig. 7-10. The equilibrium gas-phase concentrations shown in Fig. 7a correspond to the situation when crystalline silica is in equilibrium with a SiO<sub>2</sub>-rich liquid phase containing varying amounts of Na<sub>2</sub>O or K<sub>2</sub>O. Corrosion of the refractory is possible if the equilibrium calculation predicts the formation of a liquid alkali-silicate solution in equilibrium with crystalline silica as described by Reaction 2.

Figure 7a yields two important results. First, NaOH(g) is the dominant sodium-containing species and KOH(g) is the dominant potassium-containing species in the gas, significantly exceeding their respective atom concentration at all temperatures. Reaction 3 below shows how the alkali metal atom partial pressures depend not



**Figure 6.** Percent Na<sub>2</sub>O and percent K<sub>2</sub>O in these respective liquid corrosion products as a function of temperature. Crystalline SiO<sub>2</sub> is in equilibrium with these liquids.

only on the M<sub>2</sub>O activities in the glass, but also on the O<sub>2</sub>(g) partial pressures



The variations of oxygen pressure in a glass melting furnace atmosphere are not great enough to ever cause the M(g) equilibrium partial pressures to exceed those of MOH(g) species.

The predicted equilibrium concentrations of MOH(g) are always about a factor of two higher in oxy-fired furnace atmospheres than those predicted for air-fired furnace atmospheres. This is in qualitative agreement with reports that experimental concentrations of NaOH(g) in oxy-fuel furnaces are as much three to four times higher than in air-fired furnaces,<sup>2</sup> but suggests that other factors may be at work as well. The equilibrium prediction is simply a result of the differences in H<sub>2</sub>O(g) partial pressures in these two atmospheres (e.g., at 1873 K oxy-fired *p*<sub>H<sub>2</sub>O</sub> = 0.654 bar and air-fired *p*<sub>H<sub>2</sub>O</sub> = 0.177 bar). From Reaction 1 or 2, it is seen that the gaseous ratio

$$MOH_{\text{oxy}}/MOH_{\text{air}} = (H_{2O_{\text{oxy}}}/H_{2O_{\text{air}}})^{0.5} = (0.654/0.177)^{0.5} = 1.92 \quad [4]$$

Maximum MOH(g) equilibrium partial pressures occur at ~1873 K for these two systems. This results from a combination of two competing effects. The decreasing concentration (activity) of Na<sub>2</sub>O(l) in the liquid corrosion product with increasing temperature (Fig. 7b, dashed line) ultimately causes the NaOH(g) concentration to decrease at higher temperatures. Counteracting this effect, however, and leading to the maximum in the NaOH(g) concentration, is the increase with temperature in the equilibrium constant for the reaction Na<sub>2</sub>O(l) + H<sub>2</sub>O(g) ↔ 2NaOH(g) (Fig. 7b, solid line). This maximum has some interesting consequences with regard to the regions in which corrosion is predicted to occur; this is discussed in more detail below.

In addition to predicting the concentrations of sodium-containing gas-phase species, the calculations indicate that, over the 1200-2000 K temperature range of interest, *p*<sub>H<sub>2</sub>O</sub> is practically constant: 65.6 to 65.2% for oxy-fired, and 17.8 to 17.6% for air-fired fuel mixtures. This occurs because the combustion products of CH<sub>4</sub> and O<sub>2</sub>

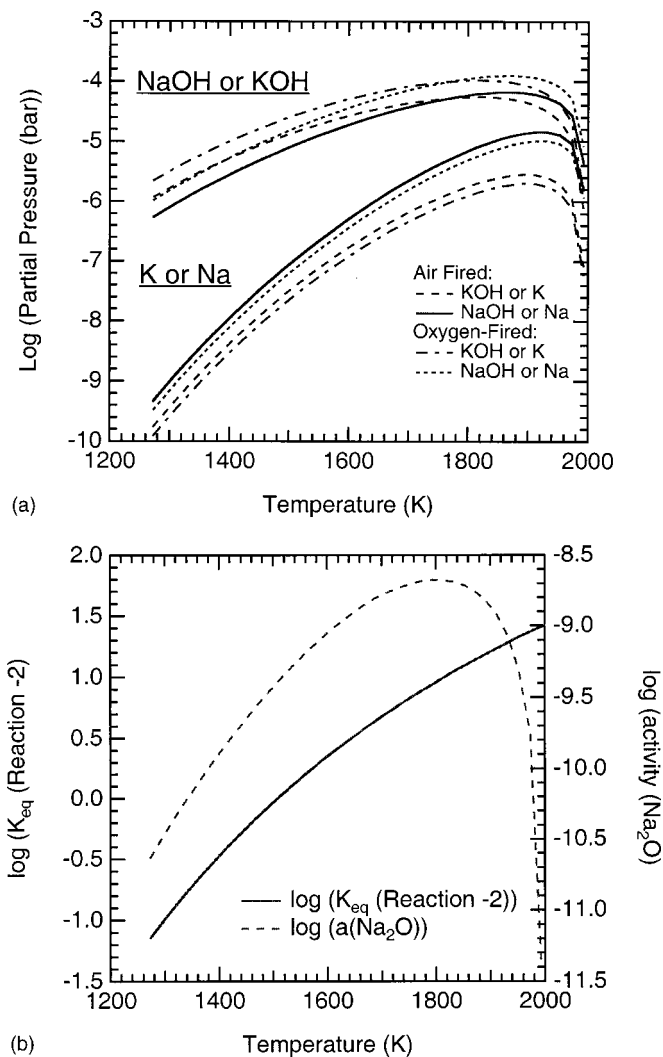


**Figure 7.** (a) Partial pressures of Na, NaOH, K, and KOH as a function of temperature for air- and oxy-fuel mixtures. The respective equilibrium water pressures produced by these fuel mixtures was 0.18 and 0.65 bar. As shown in Table I, an input O<sub>2</sub>/CH<sub>4</sub> fuel ratio of 2.05 was used. The gases were assumed to be in equilibrium with crystalline SiO<sub>2</sub> and a silica-rich liquid containing dissolved M<sub>2</sub>O. As discussed in the text, data for NaOH(g) from the JANAF Tables<sup>15</sup> were used in these calculations. (b) Temperature dependence of the equilibrium constant for Reaction 2, with the Na<sub>2</sub>O activity in the liquid phase.

are primarily CO<sub>2</sub> and H<sub>2</sub>O in this temperature range. It would thus be realistic to assume a fixed value of  $p_{\text{H}_2\text{O}}$  at all temperatures of interest.

It should also be pointed out that, under actual furnace conditions,  $p_{\text{H}_2\text{O}}$  may actually be lower than the values used here. This can be caused by the dilution of the combustion gases by gases such as CO<sub>2</sub>, which evolves from the glass melt due to the decomposition of carbonate starting materials, or by the use of auxiliary oxy-fuel burners in air-fired furnaces. We do not directly account for these dilution effects since their values depend on the mixture of raw materials used to produce the glass. However, calculation of  $p_{\text{NaOH}}$  as a function of  $p_{\text{H}_2\text{O}}$  (Fig. 8) shows that, even with relatively wide variations in  $p_{\text{H}_2\text{O}}$ , the partial pressure of NaOH(g) at a given temperature does not vary greatly. For example, increasing  $p_{\text{H}_2\text{O}}$  from 0.51 bar to 0.75 bar at 1773 K results in only a 22% increase in  $p_{\text{NaOH}}$ .

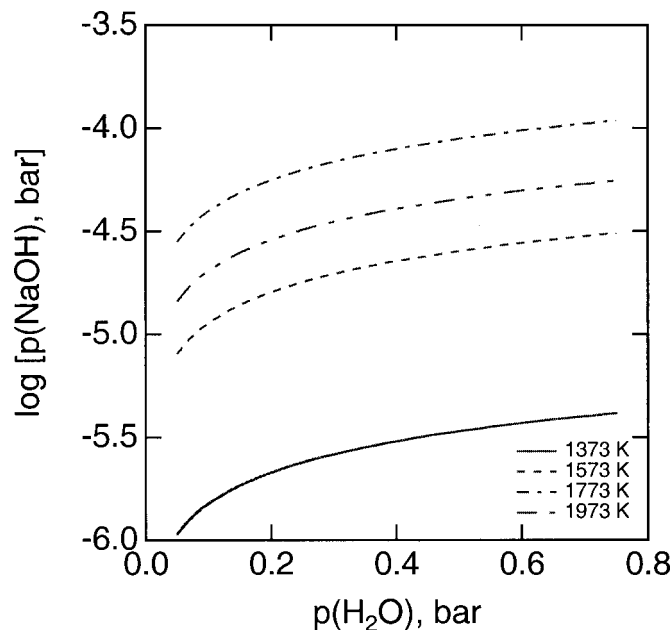


**Figure 8.** Partial pressure of NaOH as a function of H<sub>2</sub>O partial pressure for temperatures of 1373, 1573, 1773, 1973 K (1100, 1300, 1500, 1700°C). The gases were assumed to be in equilibrium with crystalline SiO<sub>2</sub> and a silica-rich liquid containing dissolved M<sub>2</sub>O. JANAF data<sup>15</sup> for NaOH(g) were used.

We note here that the refractory temperature in actual glass-melting furnaces is routinely much higher than lower temperature limits shown in Fig. 6-10 for the typically insulated crown.<sup>29</sup> Temperatures as low as 650 K can occur when the cold side of the crown is not insulated, but equilibrium calculations will almost certainly be of little use at such low temperatures since the approach to equilibrium is so slow.

The curves in Fig. 9 show that, for a given  $p_{\text{NaOH}}$ , there are temperature regions in which corrosion will occur and where it will not occur. In general, corrosion occurs (*i.e.*, a liquid sodium silicate phase forms) in the region of conditions to the right of each curve. For example, if the  $p_{\text{NaOH}}$  in the combustion atmosphere is higher than that in equilibrium with crystalline silica and the liquid sodium silicate phase (the boundary line in Fig. 9), then corrosion can occur. The lower branch of the curves in Fig. 9 thus defines a ‘‘critical temperature,’’ above which corrosion does not occur for a given  $p_{\text{NaOH}}$  in the combustion atmosphere. This concept was introduced previously by Faber and Verheijn.<sup>3,7</sup> Above the lower branch of the solid curve, corrosion will not occur since  $p_{\text{NaOH}}$  is below the equilibrium value. These results are again consistent with the observations in actual furnaces, which show that insulating the cold side of the crown refractory, and thus increasing the temperature of the hot face, slows the rate of corrosion.<sup>29</sup>

It is important to note that our calculated  $p_{\text{NaOH}}$  corresponding to the critical temperatures determined by Faber and Verheijn<sup>7</sup> are considerably lower than the input  $p_{\text{NaOH}}$  values they used. In their work, Faber and Verheijn treated NaOH(g) as a reactant, using input concentrations of 60 ppm under air-fired conditions and 220 ppm under oxy-fired conditions. They also considered only the formation of crystalline sodium silicates (or their congruent melts) as corrosion products. These assumptions lead to critical temperatures of 1593 K for air-fired and 1681 K for oxy-fired furnaces. In contrast, our calculations, which include formation of a liquid corrosion product in equilibrium with SiO<sub>2</sub>, yield 17.9 ppm and 63.5 ppm, at 1593 K and 1681 K, respectively. Thus, our results suggest that the NaOH(g) concentration above which corrosion will occur at a given temperature is significantly lower than was previously predicted.

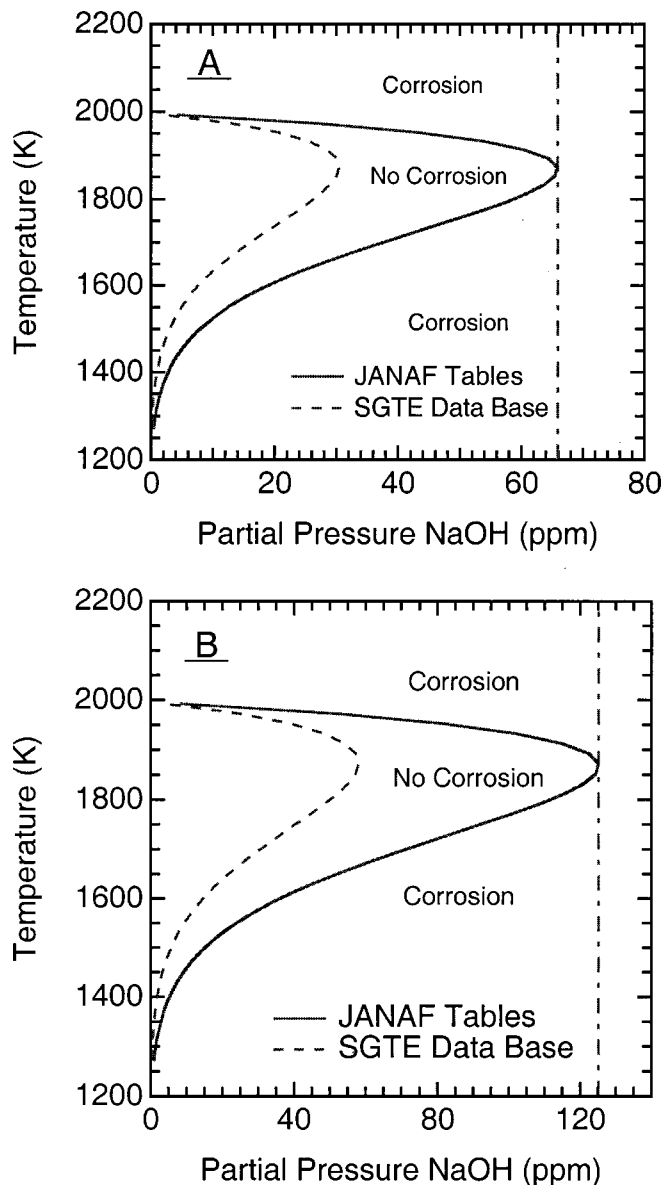


**Figure 9.** Zones of corrosion as a function of gas-phase partial pressure of NaOH, as defined by  $T_{\text{critical}}$  (see text). (A) Air-fired conditions; (B) oxy-fired conditions. Note the horizontal scales on the two plots are not the same. Data for NaOH(g) from the JANAF Tables<sup>15</sup> were used to calculate the solid curves; the dashed lines were calculated curves from using NaOH(g) data from the SGTE database<sup>14</sup> (see text). The differences in the two curves indicates the uncertainty in the zone of corrosion caused by the uncertainty in NaOH(g) thermodynamic data. The labels “Corrosion” and “No Corrosion” apply only to the solid curves. The vertical dash-dot line indicates the partial pressure of NaOH(g) above which corrosion occurs at all temperatures.

The differences between our critical temperatures and those of Faber and Verheijn are largely due to the inclusion of the liquid corrosion phase, although the thermodynamic data for NaOH(g) and several condensed-phase species are not identical between the two investigations (Ref. 7 uses the SGTE database exclusively; exceptions to this for our study are given in Table II).

Interestingly, the results in Fig. 9 suggest that, if sufficiently high temperatures are reached (*i.e.*, above the upper branch of the curves), corrosion should resume, since the NaOH concentration will again exceed the equilibrium value. This is a direct consequence of the fact that there is a maximum in the  $p_{\text{NaOH}}$  vs. temperature curve (Fig. 7a). Practically speaking, the amount of corro-

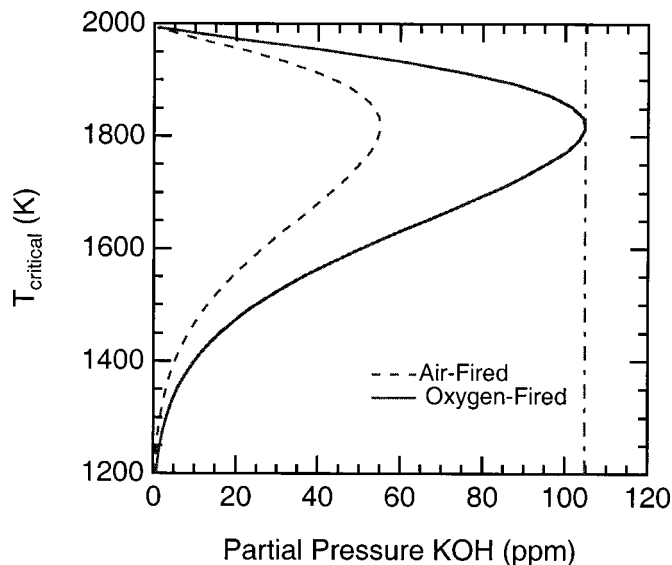


**Figure 10.** Zones of corrosion as a function of gas-phase partial pressure of KOH, as defined by  $T_{\text{critical}}$  (see text) for air- and oxygen-fired melting conditions. The vertical dash-dot line indicates the partial pressure of KOH(g) above which corrosion occurs at all temperatures.

sion might be very small at these temperatures, since the calculations reveal that the amount of  $\text{Na}_2\text{O}$  in the liquid corrosion product decreases as temperature increases (Fig. 2 and 6), leading to more viscous liquids that could pose a transport limitation to the reaction. At concentrations above  $\sim 66$  ppm (air-fired) or  $\sim 125$  ppm (oxy-fired), corrosion can occur at all temperatures since  $p_{\text{NaOH}}$  is always above the liquid- $\text{SiO}_2$  (crystalline) equilibrium value.

The two curves in Fig. 9 show that the region in which corrosion occurs shifts to higher  $p_{\text{NaOH}}$  at a given temperature as one shifts from an air-fired to an oxy-fired furnace, *i.e.*, as the concentration of water vapor in the furnace atmosphere increases. However, this result can be misleading if one does not take into account the fact that air-fired combustion atmospheres contain lower concentrations of NaOH(g) than oxy-fired atmospheres because of the higher water concentrations in the oxy-fired furnaces.

Finally, Fig. 9 shows the effect of the difference in the SGTE<sup>14</sup> and JANAF<sup>15</sup> thermodynamic values for NaOH(g) in predicting the critical boundary lines that separate corrosive from noncorrosive conditions for air-fired and oxygen-fired furnaces. This figure provides a measure of the uncertainty in quantitative numbers produced by our calculations. However, the general conclusions and explanations of the observed corrosion behavior are not dependent on the formation enthalpies of NaOH(g).

The equilibrium behavior of  $\text{K}_2\text{O}$  and  $\text{Na}_2\text{O}$  are expected to be qualitatively the same based on their similar chemical nature and this is borne out by the calculations reported here. Data for the  $\text{K}_2\text{O}$ - $\text{SiO}_2$  system are shown in Fig. 6, 7a, and 10, the first two of which also include the predictions for the  $\text{Na}_2\text{O}$ - $\text{SiO}_2$  system for direct comparison.

Figure 7a displays the predicted equilibrium partial pressures of KOH and K as a function of temperature. Like the  $\text{Na}_2\text{O}$ - $\text{SiO}_2$  system, the hydroxide is the potassium-containing species in highest concentration in the gas phase, followed by potassium atoms; no other gas-phase potassium-containing species are present in significant concentrations. The maximum  $p_{\text{KOH}}$  of  $\sim 104$  ppm under oxy-fuel conditions and  $\sim 55$  ppm under air-fuel conditions is slightly lower than  $p_{\text{NaOH}}$  and is shifted to slightly lower temperatures (1823 K for KOH vs. 1873 K for NaOH). The partial pressure of KOH is close to that of NaOH, regardless of whether air or oxygen is used. These results suggest that silica stability in atmospheres containing

KOH should be similar to that in atmospheres containing comparable amounts of NaOH.

These results suggest a mechanism that could be responsible for the phenomenon known as "ratholing," in which large voids form in the interior of the crown refractories.<sup>29</sup> These voids are typically connected to the hot face of the refractory via a narrow channel. The initial formation of the channel may be caused by relatively slow corrosion, perhaps along a joint or originating at a defect of some kind. After reaching relatively cooler regions in the interior of the refractory, however, corrosion may accelerate since there is a stronger thermodynamic driving force at lower temperatures. This driving force results from two factors: first, lower temperatures lead to lower equilibrium  $p_{\text{NaOH}}$  (Fig. 7a). Second, lower temperatures also favor liquid corrosion products containing higher concentrations of sodium (Fig. 6). As a result, if the  $p_{\text{NaOH}}$  in the channel at some point in the interior of the refractory exceeds the equilibrium value, the excess NaOH will react with the refractory to form more of the liquid-phase corrosion product, which will then reduce  $p_{\text{NaOH}}$  and increase the fraction of  $\text{Na}_2\text{O}$  in the liquid phase. As mentioned previously, increasing the concentration of sodium in the liquid phase reduces its viscosity.<sup>27,28</sup> Hence, liquid products formed at cooler temperatures may be more prone to flow back out the original entrance channel than more viscous ones formed at higher temperatures. This constant removal of reaction product could maintain a condition in which fresh refractory is continuously exposed to gas-phase NaOH, leading to continued corrosion and thus, the opening of an interior void. This mechanism, if true, confirms strategies currently used by the industry to avoid ratholing; namely, (i) insulating the back (cool) side of the refractory to minimize the temperature gradient and (ii) taking great care to avoid openings in joints through which corrosive gases can travel to cooler portions of the refractory.

### Conclusions

The results of equilibrium calculations for the  $\text{Na}_2\text{O-SiO}_2$  and  $\text{K}_2\text{O-SiO}_2$  systems are reported and indicate that the principal product of the corrosion of  $\text{SiO}_2$  refractories by gas-phase NaOH and KOH is a molten glass containing variable amounts of sodium or potassium. The amount of alkali in this product increases with decreasing temperature of the refractory. Since increasing alkali concentrations in the molten corrosion product correlate with decreasing viscosity, the results suggest that higher refractory temperatures could inhibit corrosion by promoting the formation of products that are less prone to flow away from the surface. This result confirms anecdotal evidence available from the glass manufacturing industry. The calculations also indicate that a critical temperature exists at a given alkali hydroxide partial pressure above which corrosion is not thermodynamically favored to occur, since the equilibrium hydroxide vapor pressure is higher than that existing in the furnace atmosphere. Together, these results suggest a mechanism whereby temperature gradients across the refractory crown of a glass-melting furnace could lead to formation of interior voids in the refractory (also known as "ratholing").

### Acknowledgments

We would like to thank Dr. George Pecoraro (PPG Industries, Inc.) for technical assistance in the writing of this article. For their financial support, we are grateful to the U.S. Department of Energy

(DOE) Office of Industrial Technologies Glass Industry of the Future Team; American Air Liquide, BOC Gases, PPG Industries, Inc., Praxair Inc., Techneglas, and Visteon Automotive Systems; and the DOE Environmental Management Science Program funded by the Office of Environmental Management's Office of Science and Technology, and administered jointly with the Office of Energy Research under contract DE-AC05-96OR22464 with Lockheed Martin Energy Research Corporation.

Sandia National Laboratories assisted in meeting the publication costs of this article.

### References

1. *Corrosion of Materials by Molten Glass*, G. A. Pecoraro, J. C. Marra, and J. T. Wenzel, Editors, American Ceramic Society, Westerville, OH (1996).
2. J. Boillet, C. A. Paskocimas, E. R. Leite, E. Longo, J. A. Varela, W. T. Kobayashi, and W. J. Snyder, in *Corrosion of Materials by Molten Glass*, *Ceramic Trans.* Vol. 78, G. A. Pecoraro, J. C. Marra, and J. T. Wenzel, Editors, p. 217, American Ceramic Society, Westerville, OH (1996).
3. A. J. Faber and O. S. Verheijen, *Ceram. Eng. Sci. Proc.*, **18**, 109 (1997).
4. S. J. Slade, in *Corrosion of Materials by Molten Glass*, *Ceramic Trans.* Vol. 78, G. A. Pecoraro, J. C. Marra, and J. T. Wenzel, Editors, p. 195, American Ceramic Society, Westerville, OH (1996).
5. K. T. Wu, and H. Kobayashi, in *Corrosion of Materials by Molten Glass*, *Ceramic Trans.* Vol. 78, G. A. Pecoraro, J. C. Marra, and J. T. Wenzel, Editors, p. 205, American Ceramic Society, Westerville, OH (1996).
6. H. T. Godard, L. H. Kotacska, J. F. Wosinski, S. M. Winder, A. Gupta, K. R. Selkregg, and S. Gould, *Ceram. Eng. Sci. Proc.*, **18**, 181 (1997).
7. A. J. Faber, and I. O. S. Verheijen, Report NCG-Project: Reduction of Refractory Corrosion-Phase I, TNO Institute of Applied Physics HAM-RPT-96396 (1996).
8. P. Wu, G. Eriksson, and A. D. Pelton, *J. Am. Ceram. Soc.*, **76**, 2059 (1993).
9. A. I. Zaitsev, N. E. Shelkova, N. P. Lyakishev, and B. M. Mogutnov, *Phys. Chem. Chem. Phys.*, **1**, 1899 (1999).
10. K. E. Spear, T. M. Besmann, and E. C. Beahm, *MRS Bull.*, **24**, 37 (1999).
11. K. E. Spear, and M. D. Allendorf, in *High Temperature Corrosion and Materials Chemistry*, *Proceedings of The Per Kofstad Memorial Symposium*, M. Mcmillan, E. Opila, T. Marayama, and T. Marita, Editors, PV-99-38, p. 439, The Electrochemical Society Proceedings Series, Pennington, NJ (1999).
12. G. Eriksson and K. Hack, *Metall. Trans. B*, **21B**, 1013 (1990).
13. *ChemSage™ 4.1*, GTT Technologies, Herzogonrath, Germany (1998).
14. G. Eriksson, and K. Hack, *SGTE Pure Substance Database, 1996 Version*, produced by the Scientific Group Thermodata Europe and obtained through GTT Technologies, Herzogonrath, Germany (1998).
15. M. J. Chase, Jr., *J. Phys. Chem. Ref. Data Monogr.*, **9**, 1 (1998) [NIST-JANAF Thermodynamic Tables, 4th ed.].
16. L. N. Gorokhov and A. M. Emelyanov, *Russ. J. Phys. Chem.*, **70**, 1003 (1996).
17. L. V. Gurvich, G. A. Bergman, and L. N. Gorokhov, *J. Phys. Chem. Ref. Data Suppl.*, **25**, 1211 (1996).
18. *Phase Diagrams for Ceramists*, Vol. 1-12, The American Ceramic Society, Westerville, OH (1964-1996).
19. D. A. Neudorf and J. F. Elliott, *Metall. Trans.*, **11B**, 607 (1980); data taken from Ref. 8 in this article.
20. S. Yamaguchi, A. Imai, and K. S. Goto, *Scand. J. Metall.*, **11**, 263 (1982); data taken from Ref. 8 in this article.
21. F. Tsukihashi and N. Sano, *Tetsu to Hagane*, **71**, 815 (1985); data taken from Ref. 8 in this article.
22. S. Yamaguchi, A. Imai, and K. S. Goto, *J. Jpn. Inst. Met.*, **47**, 736 (1983).
23. S. Kohsaka, S. Sato, and T. Yokokawa, *J. Chem. Thermodyn.*, **11**, 547 (1979).
24. M. G. Froberg, E. Caune, and M. L. Kapoor, *Arch. Eisenhuettenwes.*, **44**, 585 (1973); data taken from Ref. 8 in this article.
25. D. Ravaine, E. Azandegbe, and J. L. Souquet, *Silic. Ind.*, **40**, 333 (1975); data taken from Ref. 8 in this article.
26. J. M. Steiler, *Comm. Eur. Communities* [Rep.] EUR., EUR 8720 Pt. 2, p. 21, (1982); data taken from Ref. 8 in this article.
27. J. O. M. Bockris, J. D. MacKenzie, and J. A. Kitchener, *Trans. Faraday Soc.*, **51**, 1734 (1955).
28. N. P. Bansal, and R. H. Doremus, *Handbook of Glass Properties*, Academic Press, Orlando, FL (1986).
29. J. LeBlanc, *Ceram. Ind.*, **146**, 27 (1996).